Dynamic interplay of membrane-proximal POTRA domain and conserved loop L6 in Omp85 transporter FhaC

Jeremy Guérin, Nathalie Saint, Catherine Baud, Albano C Meli, Emilien Etienne, Camille Locht, Hervé Vezin, Françoise Jacob-Dubuisson

Dynamic interplay of membrane-proximal POTRA domain and conserved loop L6 in Omp85 transporter FhaC

Jeremy Guérin,[1,2,3,4] Nathalie Saint,[5] Catherine Baud,[1,2,3,4] Albano C. Meli,[5] Emilien Etienne,[6] Camille Locht,[1,2,3,4] Hervé Vezin[2,7] and Françoise Jacob-Dubuisson[1,2,3,4]*

[1]*Institut Pasteur de Lille, CIIL, 1 rue Calmette, 59019, Lille Cedex, France.*

[2]*Université de Lille, 1 rue G. Lefebvre, 59000, Lille, France.*

[3]*CNRS UMR 8204, 2 rue des Canonniers, 59046, Lille, France.*

[4]*INSERM U1019, 6 rue Pr. Laguesse, 59045, Lille, France.*

[5]*PhyMedExp, University of Montpellier, INSERM U1046, CNRS UMR9214, 371 av. G. Giraud, 34295, Montpellier cedex 05, France.*

[6]*Aix-Marseille Université, CNRS, BIP (UMR 7281), 31 chemin J. Aiguier, 13402, Marseille cedex 20, France.*

[7]*CNRS UMR8516, Bat. C4, 59658, Villeneuve d'Ascq, France.*

Summary

Omp85 transporters mediate protein insertion into, or translocation across, membranes. They have a conserved architecture, with POTRA domains that interact with substrate proteins, a 16-stranded transmembrane β barrel, and an extracellular loop, L6, folded back in the barrel pore. Here using electrophysiology, *in vivo* biochemical approaches and electron paramagnetic resonance, we show that the L6 loop of the Omp85 transporter FhaC changes conformation and modulates channel opening. Those conformational changes involve breaking the conserved interaction between the tip of L6 and the inner β-barrel wall. The membrane-proximal POTRA domain also exchanges between several conformations, and the binding of FHA displaces this equilibrium. We further demonstrate a dynamic, physical communication between the POTRA domains and L6, which must take place *via* the β barrel. Our findings thus link all three essential components of Omp85 transporters and indicate that they operate in a concerted fashion in the transport cycle.

Introduction

In Gram-negative bacteria, the outer membrane represents a major barrier for the secretion of proteins to the cell surface or the extracellular milieu. These organisms have thus developed a number of specialised secretion pathways, one of which is the Two-Partner Secretion (TPS), devoted to the export of extracellular proteins that mainly form elongated β-helices (Jacob-Dubuisson *et al.*, 2013; van Ulsen *et al.*, 2014). In TPS systems, the secreted proteins collectively called TpsA are exported across the membrane by their dedicated TpsB transporters (Jacob-Dubuisson *et al.*, 2009). The TpsB transporters belong to the Omp85 superfamily, whose members mediate the insertion of proteins into, or their translocation across, the outer membrane of prokaryotic cells or specific membranes of eukaryotic organelles (Hagan *et al.*, 2011; Schleiff *et al.*, 2011; Webb *et al.*, 2012; Selkrig *et al.*, 2014; Noinaj *et al.*, 2015).

Omp85 proteins have a modular organisation that combines soluble POTRA domains and a transmembrane β-barrel domain, with some variations around this theme (Arnold *et al.*, 2010; Heinz and Lithgow, 2014). The prokaryotic BamA and TamA insertases and the FhaC TpsB translocase have similar X-ray structures with a C-terminal, 16-stranded transmembrane β barrel that follows 5, 3 and 2 periplasmic POTRA domains respectively. A hallmark feature of the β barrel is the long extracellular loop L6 that harbours a conserved motif and is folded back in the barrel pore (Clantin *et al.*, 2007; Gruss *et al.*, 2013; Noinaj *et al.*, 2013; Ni *et al.*, 2014; Maier *et al.*, 2015). The distinct apertures of the β barrels at the extracytoplasmic side are created by specific arrangements of the extracellular loops, and they are thought to reflect the respective functions of those transporters. Thus for FhaC, the β barrel is open to the extracellular milieu for the secretion of its partner (Clantin *et al.*, 2007; Baud *et al.*, 2014; Maier *et al.*, 2015). In contrast, the position of the essential loop L6, which was recently revised for FhaC, is similar among the available structures. L6 interacts with the β barrel wall *via* a conserved salt bridge

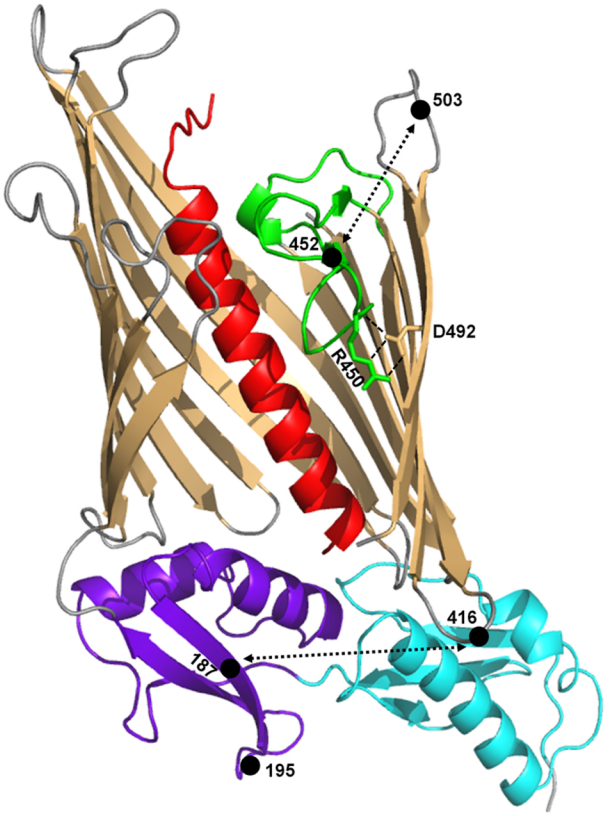

Fig. 1. FhaC structure with the positions of specific residues. The POTRA1 and 2 domains are in cyan and purple, respectively, the α-helix H1 is in red and the L6 loop in green. A cutaway view of the β barrel is presented with the positions of the spin labels marked by black dots. The pairs of residues used for PELDOR experiments are joined by stippled lines. The conserved Arg and Asp residues in L6 and B13, respectively, are also indicated with the hydrogen bonds between them. The image was created with PyMol.

between the invariant Arg of its (V/I)RG(Y/F) motif and the invariant Asp of the (F/G)xDxG motif of β barrel strand B13 (Gruss *et al.*, 2013; Noinaj *et al.*, 2013; Ni *et al.*, 2014; Maier *et al.*, 2015) (Fig. 1).

The structural conservation in the Omp85 superfamily is striking in the face of the distinct functions of its members as insertases or translocases. The molecular mechanisms of protein transport in the family remain unknown. The β barrel-proximal POTRA domain, the β barrel itself and the L6 loop are all essential for function (Bos *et al.*, 2007; Clantin *et al.*, 2007; Kim *et al.*, 2007; Delattre *et al.*, 2010; Leonard-Rivera and Misra, 2012; Noinaj *et al.*, 2013). The POTRA domains are involved in interactions with the substrate proteins, and in the case of BamA, with other proteins of the BAM complex and chaperones (Hodak *et al.*, 2006; Bos *et al.*, 2007; Bennion *et al.*, 2010; Delattre *et al.*, 2011; Ricci *et al.*, 2012; Jansen *et al.*, 2015). The β barrel serves as the protein-conducting channel (Baud *et al.*, 2014). For Omp85 transporters that function as insertases, the barrel has been proposed to open laterally to release the protein substrate into the bilayer (Gruss *et al.*, 2013; Noinaj *et al.*, 2014; Mallarino *et al.*, 2015). L6 is also hypothesised to participate in the transport mechanism. In BamA, putative L6 motions appear to be regulated by other proteins of the BAM complex (Rigel *et al.*, 2012; 2013).

FhaC of *Bordetella pertussis* is a prototypic TpsB transporter. It is dedicated to the secretion of the filamentous haemagglutinin (FHA), a major *B. pertussis* adhesin. TpsB transporters serve as translocases and work without additional factors, making them simple models for mechanistic studies of Omp85 proteins (Fan *et al.*, 2012; Baud *et al.*, 2014; Guerin *et al.*, 2014; Norell *et al.*, 2014). In addition to the features characteristic of the superfamily, TpsB transporters harbour an N-terminal helix acting as a plug for the barrel and a linker joining this helix to the first POTRA domain, POTRA1 (Fig. 1). Both H1 and this linker are highly dynamic in FhaC (Guerin *et al.*, 2014). Thus, FhaC is in equilibrium between several conformations that involve large-scale motions of the plug helix towards the periplasm, leaving the pore open for FHA translocation (Guerin *et al.*, 2014). Nevertheless, H1 is not essential for function. It most likely stabilises the resting state of the protein by its interactions with both the inner wall of the barrel and L6 (Maier *et al.*, 2015).

Conformational dynamics is thought to play a critical role for the function of Omp85 transporters. Here we use a combination of techniques to address the dynamics of the POTRA domains and L6 in FhaC. We show that L6 adopts several conformations that determine the opening state of the channel. Substrate binding to the FhaC POTRA domains affects the conformation of L6, implying a transmission of information between the periplasmic moiety and L6 *via* the β barrel.

Results

Influence of L6 on channel properties

We compared the ion-conducting profiles of selected FhaC variants with that of the wild type (wt) protein using electrophysiology to gain insight into the role of L6 for the opening states of FhaC. In response to +20 mV or –20 mV potentials, wt FhaC forms channels that display several ion-conducting states, denoted O1, O2 and O3, with conductance values centred at 300, 1050 and 1400 pS respectively (Fig. 2 and Supplementary Fig. S1). O2 is the most frequent state for wt FhaC, and the high-conductance state O3 is visited at lower frequency (Fig. 3). As blocking H1 in the pore yields channels with no or a very low conductance that may correspond to O1 (Guerin *et al.*, 2014), O2 and O3 must be open states with H1 out of the pore. Applying a low potential can thus enhance access to conformations that occur naturally.

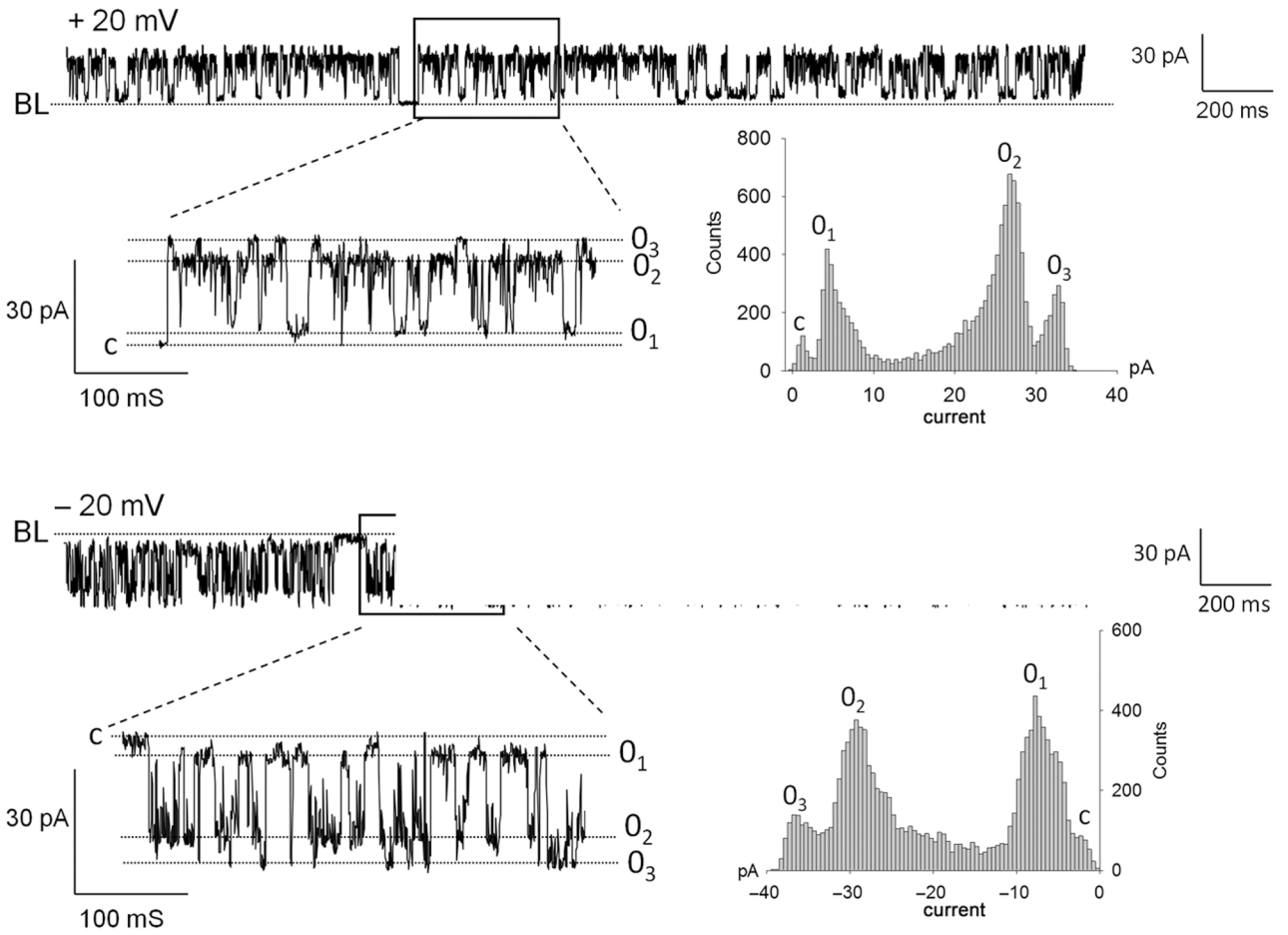

Fig. 2. Electrophysiology analyses of FhaC. Selected recordings of single-channel activity at room temperature and the associated amplitude histograms are presented for the wt protein at +20 mV and –20 mV. The three major conductance states O1, O2 and O3 identified with wt FhaC are used as references for the analysis of the FhaC variants (see Fig. 3). BL indicates the baseline. C represents the closed state of the channels.

We generated and analysed a variant of FhaC harbouring a complete deletion of L6. As expected, the $FhaC_{\Delta L6}$ variant is not functional (Supplementary Fig. S2A). It is also present in lower amounts in the cells than its wt counterpart, suggesting that L6 facilitates the biogenesis of FhaC and/or stabilises it in the outer membrane. The $FhaC_{\Delta L6}$ channels are markedly perturbed compared with the wt ones (Fig. 3). The probability for $FhaC_{\Delta L6}$ of visiting O2 is lower than for the wt protein, and O3 is hardly present at all.

To perturb the interaction between L6 and the inner wall of the β barrel while keeping the L6 loop, we altered the charges of Arg_{450} in L6 and Asp_{492} in B13, which form between them an ionic bond conserved in the Omp85 superfamily. We thus generated $FhaC_{R450D}$ and $FhaC_{D492R}$ and also combined those two substitutions to facilitate a reverse B13-L6 interaction, yielding $FhaC_{R450D+D492R}$. Unlike the L6 deletion, those polar changes do not totally abolish function (Supplementary Fig. S2). Electrophysiology shows that the channels of the three variants are altered compared with the wt channels (Fig. 3). $FhaC_{R450D}$ in particular has a very heterogeneous behaviour, with maximal and substate conductances that differ between recordings (Supplementary Fig. S3), suggesting the occurrence of metastable states.

For the three $FhaC_{R450D}$, $FhaC_{D492R}$ and $FhaC_{R450D+D492R}$ variants, the most populated conductance state at both positive and negative potentials is O1 (Fig. 3). All three have lower probabilities of visiting O2 and O3 than wt FhaC, which argues that the conserved Arg in L6 and Asp in B13 contribute to stabilising the open states of FhaC. Interestingly, O3 has lower conductance values at –20 mV for $FhaC_{R450D}$ and $FhaC_{R450D+D492R}$ than for the wt or $FhaC_{D492R}$ proteins (Supplementary Fig. S1). Conversely, the O3 state of $FhaC_{D492R}$ can reach higher levels of conductance than wt FhaC at –20 mV, albeit at low frequency (Supplementary Fig. S3). The observation that the replacement of Asp_{492} enables FhaC to achieve a wider

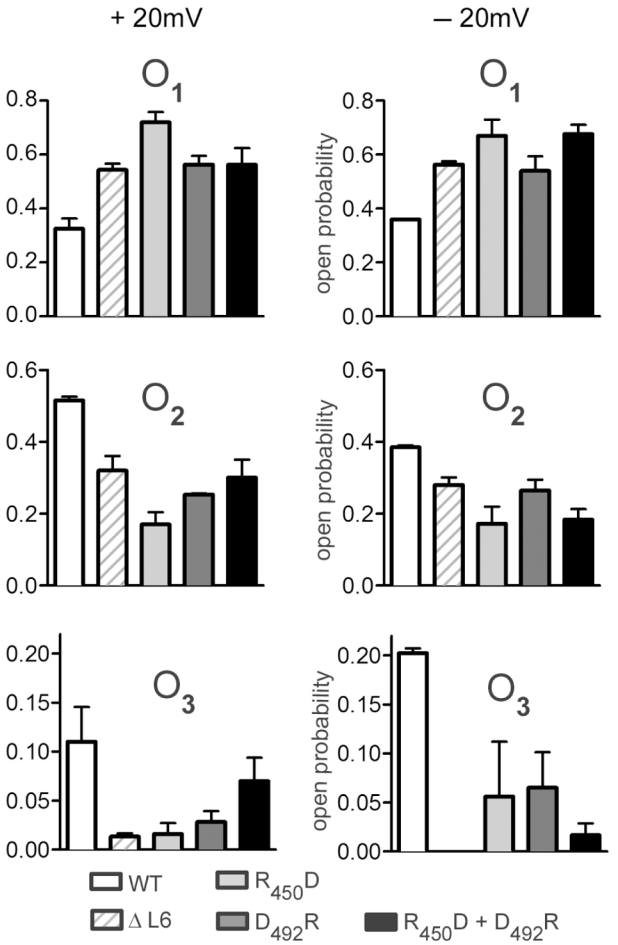

Fig. 3. Channel properties of FhaC variants. The open probabilities (Po) represent the frequencies of opening to the O1, O2 and O3 levels of conductance as defined in Fig. 2. They are shown for wt FhaC (white bars) $FhaC_{\Delta L6}$ (striped bars), $FhaC_{R450D}$ (light grey bars), $FhaC_{D492R}$ (dark grey bars) and $FhaC_{R450D+D492R}$ (black bars) at +20 mV and –20 mV. Three to five recordings of several seconds (15 to 60 s) were used for each protein at the two potentials to calculate the Pos. The Po to the O3 state for $FhaC_{\Delta L6}$ at –20 mV is < 0.01. The deletion of L6 previously characterised (Clantin *et al.*, 2007) also encompassed part of the β-barrel strand B12, while that presented here is based on the recently revised structure of FhaC (pdb # 4QKY). Note that the vertical scale differs between the O1, O2 and O3 panels.

open state suggests the occurrence of alternative conformations of L6, in which at least Arg_{450} might interact with residue(s) other than Asp_{492}.

We also assessed the role of L6 *in vivo* by performing antibiotic sensitivity assays with the FhaC variants as described (Clantin *et al.*, 2007). Larger zones of growth inhibition than for wt FhaC are observed for all four mutants (Supplementary Fig. S2B). This effect is particularly conspicuous for $FhaC_{D492R}$, which also displays the largest spikes of conductance *in vitro* (Supplementary Fig. S1). The antibiotic sensitivity of the $FhaC_{R450D+D492R}$ variant is more similar to that of wt FhaC than the single variants (Supplementary Fig. S3).

Thus, FhaC adopts several states of opening, and the presence and position of L6 in the β barrel strongly affect the channel properties. The electrophysiology data also indicate that in addition to positioning L6 in the β barrel in the resting state of the transporter, the conserved Arg in L6 and Asp in B13 might have other roles or partners.

In vivo, *FHA-dependent and -independent motions of L6*

We investigated the putative *in vivo* motions of L6 from its 'resting' position in the β barrel by specifically labelling FhaC from the bacterial surface with a 5 kDa sulfhydryl-specific reagent, PEG-MAL. We used FhaC variants each harbouring a unique Cys residue in L6 and previously shown to be functional using a secretion assay developed in *Escherichia coli* (Baud *et al.*, 2014; Guerin *et al.*, 2014). Following treatment of the bacteria with PEG-MAL, the cells were lysed, and FhaC was detected by immunoblotting. When FhaC is expressed alone, a weaker band corresponding to the FhaC-PEG adduct occurs in addition to the expected one for the variants with a Cys at positions 446, 456 and 459 (Fig. 4). The small proportions of labelled species suggest that L6 might not adopt the same conformation in all molecules, and/or that the efficiency of the labelling reaction is low. We performed the same experiments with bacteria that coexpress FhaC and an Fha30-BugE chimera mimicking a translocation intermediate (Guerin *et al.*, 2014). The chimera engages into FhaC across the outer membrane but stalls, with its FHA moiety accessible from the cell surface and its globular BugE moiety in the periplasm, thus creating a blocked complex that provides access to the conformation of FhaC 'in action'. The FhaC adducts disappear for the previously labelled positions, whereas new ones are detected for Cys at positions 448 and 452 (Fig. 4). The proportions of modified protein are again low, suggesting that L6 also adopts several conformations when FhaC is translocating FHA. A larger species migrating at the expected position for a dimer of $FhaC_{C452}$ appears in the presence of the chimera. While we have no evidence that dimerisation is relevant to function, accumulation of the cross-linked dimer over the induction period of the chimera indicates that the tip of L6 is at the cell surface and mobile when FhaC translocates FHA. Thus, the fact that L6 moves out of the pore in the course of FHA translocation argues that the Arg_{450}-Asp_{492} salt bridge between L6 and B13 breaks at some point in the transport cycle.

We combined the Arg_{450}Cys substitution at the tip of L6 with the Asp_{492}Cys one in B13, or with substitutions to Cys of extracellular residues, i.e. 218 at the end of β-barrel strand B1, 391 in the extracellular loop L5 and 503 in the extracellular loop L7, to probe the spontaneous formation

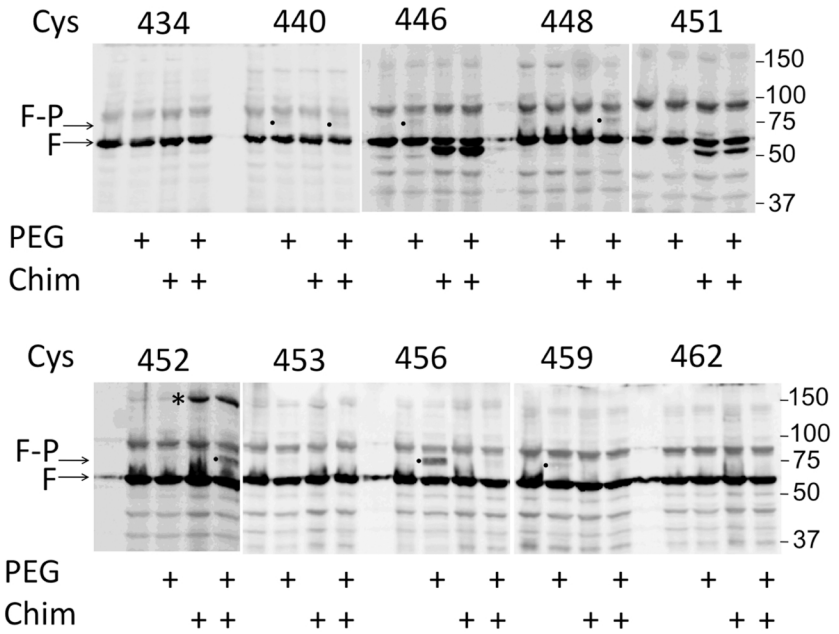

Fig. 4. *In vivo* labelling of FhaC. Bacteria expressing the $FhaC_{Cys}$ variants, as indicated by the position of the Cys residue, were treated with PEG-MAL (5K). FhaC was expressed alone or with Fha30-BugE (denoted chim). The PEG-FhaC adduct is denoted F-P and marked with a small black dot at the left of each relevant band, while F indicates the non-modified FhaC. The slow-migrating band of $FhaC_{C452}$ that likely corresponds to a dimer is indicated with an asterisk. That species is DTT-sensitive (not shown). The blot was probed with anti-FhaC antibodies.

of *in vivo* disulfide (S-S) bonds in liquid culture conditions as described (Guerin *et al.*, 2014). This was performed in a *dsbA*$^-$ background to ensure that the potential intramolecular S-S bonds do not form in the periplasm during FhaC biogenesis. Because the putative cross-linked forms should accumulate over time, they might be detected even if the alternative positions of L6 naturally occur at low frequency. The cells were treated with N-ethylmaleimide to block the free sulfhydryl groups before lysis and immunoblotting. In non-reducing conditions, an additional band with an aberrant migration is detected in several cases (Fig. 5). Cys_{450} at the tip of L6 cross-links with Cys_{492} in the barrel wall as expected, but also with Cys residues at the extracellular positions 218 and 503, but not at the periplasmic position 86 used as a control. Notably, those *in vivo* S-S bonds form without the coexpression of FHA or the chimera. Therefore, L6 spontaneously adopts alternative conformations, even though they probably represent minor forms of FhaC in the absence of FHA. While the dynamics of L6 when it is out of the pore makes it possible for residue 450 to be close to those surface residues, the L6 conformations captured in these experiments may not all be functionally relevant.

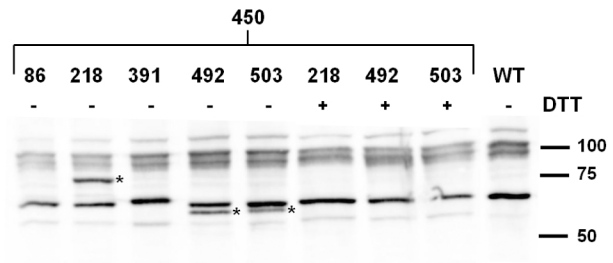

Fig. 5. *In vivo* localisation of L6 probed by spontaneous S-S bond formation. The FhaC variants with one Cys residue at position 450 and another one at each of the indicated positions were detected by immunoblotting of membrane extracts with anti-FhaC antibodies. The asterisks indicate species with an aberrant migration because of an intramolecular S-S bond. The reducing agent DTT was added where indicated. The Cys-less, wt protein is shown as a control. The experiments were performed in *dsbA*$^-$ bacteria. Note that the production of some variants, in particular $FhaC_{C450+C492}$, is toxic to wt bacteria, most likely because S-S bond formation in the periplasm hampers the insertion of the protein into the outer membrane. $FhaC_{C450+C492}$ is not functional.

FHA–FhaC interactions affect L6

The first step of the transport cycle corresponds to the recognition of FHA by the POTRA domains in the periplasm. To determine whether the binding of FHA is signalled to L6, we performed site-directed spin labelling coupled to continuous-wave electron paramagnetic resonance (CW EPR) experiments. The CW EPR spectra reflect the mobility of the paramagnetic label grafted to the protein and thus the local environment of the label. This mobility is very sensitive to structural changes and is characterised by a correlation time, τ_c (Hubbell *et al.*, 1996). Single Cys variants of FhaC were purified and labelled in a site-specific manner using the sulfhydryl-specific reagent MTSL. The modified Cys side-chain is called R1. The CW spectra were recorded for labelled FhaC reconstituted in small unilamellar vesicles (SUVs), alone or in the presence of FHA, as described (Guerin *et al.*, 2014).

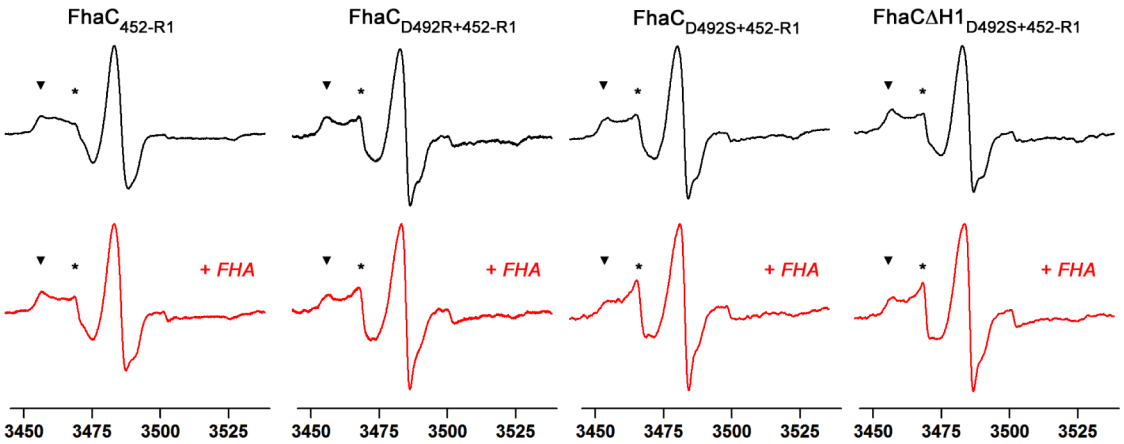

Fig. 6. CW-EPR analyses of FhaC with a spin label in the loop L6. Normalised spectra of $FhaC_{452\text{-}R1}$ with the indicated substitutions, alone or mixed with $Fha30_{N66I}$ (denoted '+FHA'), are shown. ΔH1 indicates an FhaC variant with a deletion of the N-terminal α-helix H1. The experiments were performed in SUVs. The slow and fast spectral components are indicated by an arrowhead and an asterisk respectively. The magnetic field is in Gauss. The simulations of the spectra with the occupancy of each state are shown in Supplementary Fig. S4.

The spectrum of the $FhaC_{452\text{-}R1}$ variant with a spin label in L6 shows a slow mobility of the label (Fig. 6), consistent with earlier observations (Guerin *et al.*, 2014). This spectrum can be simulated with four components: a very slow component, with a correlation time $\tau_c = 130$ ns (represented at 13%), two majority, intermediate components of $\tau_c = 7.0$ ns (49%) and $\tau_c = 2.9$ ns (37%) and a fast component with $\tau_c = 0.4$ ns (< 1%) (Supplementary Fig. S4). Note that this fast component differs from the free label in solution. This complex spectrum indicates that L6 adopts a range of constrained conformations. To enhance the potential motions of L6, we altered the connection between L6 and the β-barrel strand B13 by replacing Asp_{492} with Ser or Arg. The spectra of $FhaC_{D492S+452\text{-}R1}$ and $FhaC_{D492R+452\text{-}R1}$ consist in the same four components, with somewhat different distributions than that of $FhaC_{452\text{-}R1}$ (Fig. 6 and Supplementary Fig. S4). This suggests that the conserved Asp–Arg interaction cannot be the only reason for the slow mobility of L6. We then added to the three variants a model substrate protein, $Fha30_{N66I}$ (thereafter called FHA) that comprises the N-terminal 'TPS' domain recognised by FhaC (Hodak *et al.*, 2006; Guerin *et al.*, 2014). In all three cases the addition of FHA modifies the spectra in a highly reproducible manner. The effects are most visible for $FhaC_{D492S+452\text{-}R1}$. Thus, the proportions of the fast-mobility spectral components increase in the presence of FHA, while that of the rigid component decreases (Fig. 6 and Supplementary Fig. S4). The same effect is observed in the absence of the α-helix H1 (Fig. 6), indicating that it is independent of the position or motions of H1. Thus, although the effects are modest, binding of FHA to the POTRA domains affects L6 dynamics. Our results however argue against a direct interaction between FHA and L6, in which case one would expect a decrease in L6 mobility. Therefore, the effects of FHA binding on L6 mobility are likely indirect.

To better define the changes involved we introduced two spin labels at positions 452 in L6 and 503 in the extracellular loop L7 for pulsed electron double resonance (PELDOR) spectroscopy experiments, as described (Guerin *et al.*, 2014). Thus, by placing two spin labels in the same protein one can obtain distance information between them. Because PELDOR is performed at 50 K, the sample is frozen in the conformation(s) represented at a given time in the FhaC population. Efficient labelling at both sites together was obtained in the absence of H1. The distances extracted from the $FhaC_{452\text{-}R1+503\text{-}R1}$ PELDOR signals, centred at 3 and 3.9 nm, are longer than the 2 and 2.5 nm distances predicted by simulations of the MTSL rotamers based on the X-ray structure (Fig. 7 and Supplementary Fig. S5). In the presence of FHA, a distance centred at 2.3 nm appears, close to the expected distances, whereas the former two distance distributions are displaced to somewhat higher values. These changes show that binding of FHA to the POTRA domains affects the position of L6.

Altogether, thus, the EPR data indicate L6 adopts an ensemble of conformations, and FHA binding to the POTRA domains enhances specific conformation(s) of L6. Note that these *in vitro* experiments probe the initial step of the transport cycle that involves molecular recognition between the two partners, but not the translocation step that follows FHA binding *in vivo*. Therefore, the state of the POTRA domains influences that of L6 even though the two regions do not interact directly, and signalling from the POTRA domains to the L6 loop occurs before FHA engages into the channel.

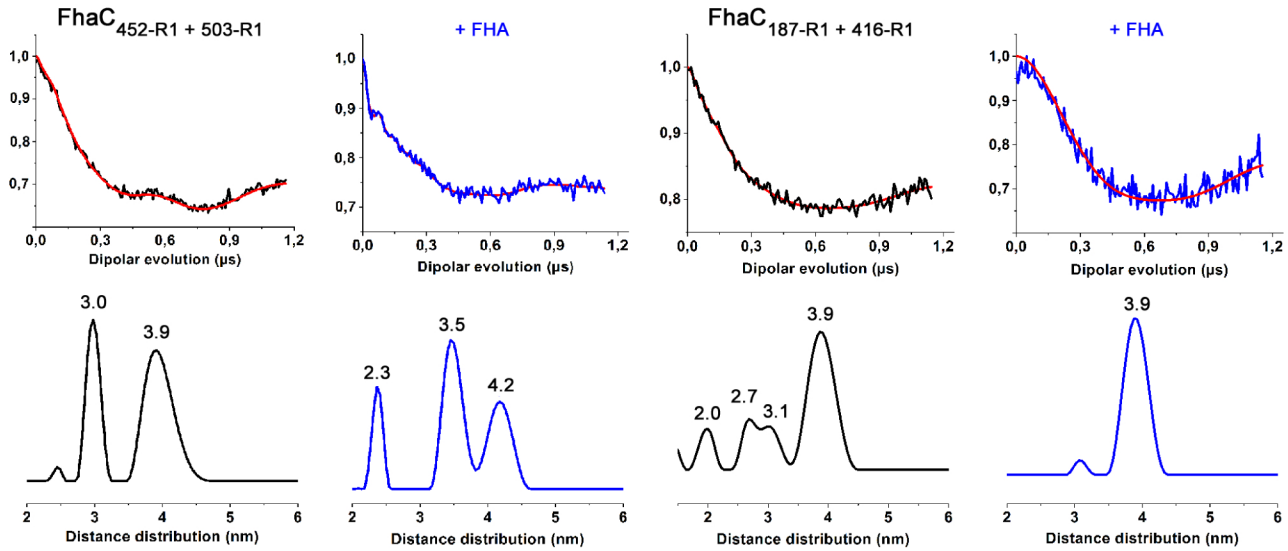

Fig. 7. PELDOR analyses. Dipolar evolution after background subtraction (upper panels) and distance distributions (lower panels) for FhaCΔH1$_{452\text{-}R1+503\text{-}R1}$ and FhaC$_{187\text{-}R1+416\text{-}R1}$ in SUVs, alone or with FHA. The distances predicted between the spin labels are shown in Supplementary Fig. S5.

Influence of FHA and L6 on POTRA2

We next tried to determine whether, reciprocally, the state of L6 might affect that of the POTRA domains. We first investigated the mobility of the POTRA domains by labelling FhaC with MTSL at position 195 in the short loop between the second and third β strands of the POTRA2 β sheet, b5 and b6 (Fig. 1) and by performing CW-EPR analyses. Notably, the spectra of FhaC$_{195\text{-}R1}$ are very different depending on the milieu. The mobility of the spin label in detergent is rapid (92% with $\tau_c = 4.2$ ns and 8% with $\tau_c = 0.5$ ns), as expected from a solvent-exposed loop region (Fig. 8). In contrast, for FhaC$_{195\text{-}R1}$ in SUVs, a new, slower component appears ($\tau_c = 7.6$ ns), whose weight decreases by approximately 40% in the presence of FHA (83% without FHA and 46% with FHA) (Fig. 8 and Supplementary Fig. S4). The low-mobility spectral component for FhaC$_{195\text{-}RI}$ in SUVs corresponds to a highly constrained spin probe, in a state of the POTRA2 domain not detected in detergent. The binding of FHA to FhaC favours a state of the POTRA2 domain in which the motions of the spin probe in the b5-b6 loop are unhindered, similar to the mobility detected in detergent (Fig. 8 and Supplementary Fig. S4). Thus, the POTRA domains appear to naturally exchange between several conformations. By binding to FhaC, FHA selects a specific conformation.

To gain additional insight into the positions of the POTRA2 domain relative to the β barrel, we also performed PELDOR spectroscopy experiments. Labels were introduced at positions 187 in the edge b5 strand of the POTRA2 domain (Guerin *et al.*, 2014) and 416 in the intracellular turn between B10 and B11 of the β barrel.

Fig. 8. CW-EPR analyses of FhaC with a spin label in the POTRA2 domain. Normalised spectra of FhaC$_{195\text{-}R1}$ and of the variant carrying the Asp$_{492}$Arg substitution are shown. The spectra at the top are those of the two proteins in detergent (denoted dtg). The other four are of the proteins reconstituted in SUVs (denoted lip), alone or with Fha30$_{N66I}$ added (denoted + FHA). The slow and fast spectral components are indicated by an arrowhead and an asterisk respectively. The magnetic field is in Gauss. The simulations of the spectra with the occupancy of each state are shown in Supplementary Fig. S4.

Simulation of the rotamers for $FhaC_{187\text{-}R1+416\text{-}R1}$ predicts a distance between the spin labels of approx 3.6 nm (Supplementary Fig. S5). Several distances were extracted from the PELDOR signals, one centred at 3.9 nm in the expected range, but also shorter ones from 2 to 3.1 nm, supporting the idea that the POTRA domains adopt more than one conformation relative to the β barrel. When FHA is added to FhaC, the shorter distances disappear, while the 3.9 nm distance remains prominent. This confirms that FHA binding to the POTRA domains affects the equilibrium of conformations of the FhaC periplasmic moiety. It appears to favour a conformation similar to that in the X-ray structure, in which the POTRA2 domain is accessible from the periplasm.

Finally, we introduced the $Asp_{452}Arg$ substitution in $FhaC_{195\text{-}R1}$ to break the ionic interaction between L6 and the β barrel, as occurs at some stage of the transport cycle, and we determined the effect on the CW-EPR spectrum. In detergent, the spectrum of $FhaC_{D492R+195\text{-}R1}$ has a more prominent fast component ($\tau_c = 0.5$ ns) than that of $FhaC_{195\text{-}R1}$, and similar to the latter it displays no rigid component. In SUVs, the proportions of the fast and low-mobility components are different for $FhaC_{D492R+195\text{-}R1}$ and for $FhaC_{195\text{-}R1}$ (Fig. 8 and Supplementary Fig. S4). This shows that the state of L6 affects that of the POTRA2 domain. FHA has a limited effect on the spectrum of $FhaC_{D492R+195\text{-}R1}$, probably because the $Asp_{492}Arg$ substitution by itself increases the mobility of the POTRA2 domain (Fig. 8 and Supplementary Fig. S4). Therefore, the data show that the communication between the L6 loop and the β barrel-proximal POTRA domain is bidirectional.

Discussion

L6, the membrane-proximal POTRA domain and the β barrel are conserved and essential for function (Bos *et al.*, 2007; Clantin *et al.*, 2007; Kim *et al.*, 2007; Leonard-Rivera and Misra, 2012; Noinaj *et al.*, 2013), and their dynamics have been suggested to participate in the mechanism of Omp85 transporters (Noinaj *et al.*, 2013). Here, we show that the POTRA2 domain and the L6 loop of FhaC both exchange between several conformations. FHA performs a conformational selection in favour of a binding-competent form of FhaC in which the POTRA domains presumably extend away from the β barrel. FHA binding to the POTRA domains affects L6. Interestingly, altering the conserved Arg–Asp interaction between L6 and the B13 strand of the barrel also affects the POTRA2 domain, which indicates a two-way communication between them. Because P2 and L6 are not close to each other in FhaC, the respective states of the POTRA domains and L6 must signal to one another *via* the β barrel itself. Our findings thus link all three essential components of Omp85 transporters.

The Arg–Asp salt bridge interaction between L6 and the B13 strand of the barrel wall is present in the available Omp85 structures – i.e., those of BamA, TamA and FhaC – and therefore it is likely a conserved feature of the superfamily (Gruss *et al.*, 2013; Noinaj *et al.*, 2013; Ni *et al.*, 2014; Maier *et al.*, 2015). Nevertheless, here we demonstrate the conformational heterogeneity of FhaC's L6 *in vitro* and *in vivo* and provide evidence that some of its conformations involve the spontaneous disruption of the Arg–Asp interaction between L6 and the β barrel wall. These alternative L6 conformations occur in the absence of FHA, as the *in vivo* formation of S-S bonds between the L6 tip and surface loops attest. When FhaC is translocating FHA, the L6–barrel wall interaction is interrupted. Thus, making and breaking the interaction between the tip of L6 and the wall of the β barrel are part of the transport cycle.

Interestingly, disruption of the L6–b13 interaction appears to have a less dramatic impact on FhaC than on BamA. Thus, it is critical for the proper folding of BamA and to stabilise the barrel structure most likely in the resting state (Noinaj *et al.*, 2013; Ni *et al.*, 2014). In contrast, for FhaC, this interaction does not appear to significantly contribute to barrel stability, and when the conserved Arg or Asp are replaced by polar residues, the function of the transporter is partly preserved (this work). A noticeable difference between the two proteins is the presence of the N-terminal α-helix in the FhaC barrel pore (Maier *et al.*, 2015). This N-terminal helix is a conserved feature of TpsB transporters that is not found in other Omp85 proteins (Guerin *et al.*, 2014). In the resting state of the FhaC channel, H1 makes several interactions with the barrel wall and with L6, which may account for the increased stability of the barrel if the L6–b13 interaction is disrupted by mutagenesis.

The two structural elements that obstruct the pore of FhaC, L6 and H1, both undergo large conformational changes in the secretion cycle (Guerin *et al.*, 2014 and this work). The respective *in vivo* motions of H1 and L6 most likely influence one another. Electrophysiology experiments strongly argue that in the open states O2 and O3 of FhaC, H1 is out of the pore (Méli *et al.*, 2006; Guerin *et al.*, 2014; and this work). Those two states thus correspond to distinct conformations of FhaC involving L6 and the β barrel. The dynamics of L6 strongly affect the properties of the FhaC channels, and we propose that the motions of L6 regulate the opening states of FhaC for function. In particular, the L6 motion towards the cell surface may facilitate the exit of H1 and the progression of FHA in the channel. Arg_{450} at the tip of L6 probably forms alternative interactions in the open state(s) of FhaC, and it is conceivable that the conserved Asp_{492} in the β barrel also has other interaction partners in the transport cycle.

The POTRA2 domain adopts several conformations, in one of which the loop between b5 and b6 in the POTRA β sheet appears to be strongly constrained. While substrate recognition is an established function of the POTRA domains (Hodak *et al*., 2006; Delattre *et al*., 2011; Baud *et al*., 2014), the involvement of at least the membrane-proximal POTRA domain in the transport cycle most likely goes beyond. The reorientation of the POTRA2 domain relative to the barrel in the transport cycle may regulate FHA access to, and promote its progression into, the FhaC channel. The dialogue between the POTRA2 domain and L6 argues that they operate in concert in the course of the secretion cycle. In FhaC, there is a network of interactions between the POTRA2 domain, the periplasmic loop that connects β-barrel strands B6 and B7 and the linker that connects H1 and the POTRA1 domain (Maier *et al*., 2015). This network might form a signalling path between the POTRA domains and L6 *via* the β barrel. Taking part in this network is Asp_{173} in the second helix of POTRA2, which is conserved among TpsB proteins and critical for FhaC function but not for FHA recognition (Delattre *et al*., 2011). The linker between H1 and the POTRA1 domain is also essential for FhaC function (Guedin *et al*., 2000). It partially covers the FHA binding site along the POTRA2 domain in the resting state of the transporter and must therefore be displaced early in the transport cycle. The breaking of the linker-POTRA-barrel interaction network for substrate recognition by the POTRA domains might serve as a signal to the β barrel, thus triggering further conformational changes necessary for the transport cycle.

Our study of FhaC identifies motions similar to those suggested for other Omp85 proteins. Thus, two different BamA structures have led to the hypothesis that putative motions of the POTRA domains and of L6 relative to the β barrel may be conformational switches related to function (Noinaj *et al*., 2013). Our demonstration of a dynamic, physical link between the POTRA2 domain and the L6 loop also confirms suppressor mutant and co-variance analyses that have indicated a functional connection between the POTRA domains and L6 in BamA (Tellez and Misra, 2012; Dwyer *et al*., 2013). The successive conformational states of the Omp85 transporters in their mechanistic cycle are thus notably mediated by the membrane-proximal POTRA domain and the L6 loop. That this should be true for both insertases like BamA and translocases like FhaC strongly implies common mechanisms for Omp85 transporters.

We thus propose the following mechanistic model for FhaC. The transporter naturally interchanges between several conformations that involve motions of H1 and the linker, of the POTRA domains and of L6. The conformational exchanges occur in the absence of FHA, although the resting state probably predominates in that case. The different conformations of L6 give rise to distinct opening states of the channel. The incoming FHA substrate selects a form that is open on the periplasmic side, with H1 out of the pore and the hydrophobic groove along the β sheet of the POTRA2 domain accessible for binding (Guerin *et al*., 2014). Following FHA binding, swing motions of the POTRAs and conformational changes of L6 facilitate entrance of a segment of the extended FHA polypeptide into the channel. After delivering this first load to the channel the POTRA domains release the portion of FHA that they are holding and return to the periplasmic-open conformation for the cycle to resume with a following segment of FHA. When FHA emerges at the extracellular surface it binds to the β sheet formed by the long B5-B8 β strands of FhaC protruding from the membrane, probably by β augmentation (Baud *et al*., 2014), and the FHA β helix starts to fold. The conformational cycle of FhaC proceeds in a repetitive manner until FHA has folded a sufficiently long portion of its β helix at the cell surface to prevent backsliding, thus conferring directionality on the translocation process. An important question remains regarding the nature of potential conformational changes of the β barrel itself (Noinaj *et al*., 2014). Finally, as there is no energy available in the periplasm or the outer membrane to power conformational changes, the distinct conformations of FhaC should have similar free energy levels, with low energy barriers between them.

Experimental procedures

Plasmids

All the mutations in *fhaC* were generated using the QuikChange II XL Kit (Agilent Technologies) on pFc3, which expresses *fhaC* under the control of a weak constitutive promoter (Guedin *et al*., 2000). For overproduction and purification of FhaC in *E. coli*, the *Bam*HI-*Hin*dIII fragments from the pFc3 variants harbouring a Cys codon were exchanged for their wt counterpart in pT7FcW (Clantin *et al*., 2007). For the electrophysiology experiments the FhaC variants were produced with an N-terminal 6-His tag, as described earlier (Méli *et al*., 2006). The model substrate, $Fha30_{N66I}$, was produced in *E. coli* from $pHod6N_{66}I$ (Hodak *et al*., 2006). The Fha30-BugE chimera was described (Guerin *et al*., 2014). pTac138NM2-LkH codes for the FHA model protein used for the secretion assays in *E. coli*, Fha60, a 60 kDa N-terminal truncate of FHA followed by a Gly-Ser linker and a 6-His tag. To construct pTac138NM2-LkH, a linker coding for a 6-His motif was inserted into *Bam*HI- and *Hin*dIII-restricted pEC138b (Alsteens *et al*., 2013), yielding pEC138bHΔ. The 508 bp *Not*I-*Bam*HI fragment of the latter was replaced with the 1430 bp fragment from pEC138HisN-NM2-LX2C (Alsteens *et al*., 2013). A second linker coding for a stretch of 8 Gly-Ser in tandem was inserted into *Bam*HI of the resulting plasmid. From the latter, the 2080 bp EcoRI-HindIII fragment was excised and introduced into pBBiTac (Alsteens *et al*., 2013), yielding pTac138NM2-LkH.

Protein purification and spin labelling

The purification of the FhaC derivatives was performed as described (Clantin *et al*., 2007) except that 3 mM tris(2-carboxyethyl)phosphine (TCEP, Sigma) was added to the detergent extract before ion exchange chromatography to prevent S-S bond formation *in vitro*. The FhaC-containing fractions were pooled and immediately mixed with a 10-fold molar excess MTSL (Toronto Research Chemicals). The labelling reaction was performed at room temperature with gentle agitation for 4–8 h, after which the mixture was diluted 10 folds and subjected to cation-exchange chromatography in 0.8% Elugent. Spin-labelled FhaC was eluted with a 600 mM NaCl pulse. The FHA fragment used as the substrate of FhaC for the *in vitro* experiments was $Fha30_{N66I}$, to prolong the extended conformation of the TPS domain necessary for interaction with FhaC (Hodak *et al*., 2006; Delattre *et al*., 2011). It was produced in *E. coli* BL21(DE3) and purified in urea by metal chelate chromatography as described in Hodak *et al*. (2006), concentrated to 13 mg ml^{-1} in 6 M urea and stored at 4°C.

Liposome preparation and protein reconstitution

Escherichia coli Polar lipids (Avanti) solubilised in chloroform (50 mg in 6 ml) were evaporated under argon. The pellet was suspended in 10 ml 50 mM Tris-HCl (pH 7.5) and sonicated in a bath. The liposomes were extruded through a 100-nm-pore polycarbonate membrane (Sigma), and the resulting SUVs were mixed with FhaC (16:1; w/w) at room temperature, with gentle agitation for 1 h. The proteoliposomes were formed by removal of detergent with the progressive addition of wet Biobeads SM2 (Bio-Rad) to 40 mg ml^{-1}, under gentle agitation. The beads were removed, and the proteoliposomes were collected by ultracentrifugation at 150 000× *g* for 1 h at 12°C and resuspended in 450 µl of 50 mM Tris-HCl (pH 7.5). All the steps were performed under argon.

EPR experiments

Spin-labelled FhaC at about 60 µM was injected into a quartz flat cell with a useful volume of 100 µl. CW-EPR spectra were recorded at room temperature (296 K) on an ESP 300E Bruker spectrometer equipped with an ELEXSYS Super High Sensitivity resonator operating at 9.8 GHz, and the microwave power was set to 10 mW, with a magnetic field modulation frequency of 100 kHz, and the amplitude of 0.1 mT. The samples were recorded with 5–15 accumulation spectra depending on spin labelling efficiency. $Fha30_{N66I}$ (30 µl of a 330 µM solution in 6 M urea) was added where indicated. The simulation of the CW-EPR spectra was performed with the Easyspin software package under Matlab (Stoll and Schweiger, 2006). The spectra were normalised for presentation.

PELDOR experiments were performed at 50 K with a Bruker ELEXSYS E580 X band spectrometer using the standard MD5 dielectric resonator and equipped with an Oxford helium temperature regulation unit. The T2 transverse relaxation time measured using 2-pulse-echo Hahn decay for each sample was used to evaluate the dipolar time domain extent allowed for distance measurements. The experiments were performed using the four-pulse DEER sequence $(\pi/2)\nu_1$-τ_1-$(\pi)\nu_1$-τ-$(\pi)\nu_2$-$(\tau_1 + \tau_2)$-τ-$(\pi)\nu_1$-τ_2-echo (Jeschke, 2002). The pump pulse (ν_2) length was set to 20 ns and applied at the maximum of the left part of the spectrum with the optimisation of the amplitude set to the maximum of echo inversion. The observer pulses (ν_1) $\pi/2$ and π lengths were set respectively to 16 and 32 ns and positioned at a 70 MHz higher frequency. As T2 is very short (0.6–1.2 µs), the τ_1 value was set to 136 ns for short T2 and to 200 ns for higher ones in order to maximise the signal-to-noise ratio. τ_2 was set to 1.2 µs due to these short T2 values. We previously verified that the echo decay for FhaC with a single spin label does not display any oscillations (Guerin *et al*., 2014). Signal processing was achieved using the DeerAnalysis2011 software package under Matlab (Jeschke *et al*., 2006). The signal was corrected by subtracting the un-modulated background echo decay using a homogeneous three-dimensional spin distribution. The Tikhonov regularisation was applied to the corrected dipolar evolution data set to obtain the distance distributions (Tikhonov and Arsenin, 1977). Calculations of the expected distances based on the X-ray structure of FhaC (pdb 4qky) were performed using the molecular mechanics software MMM (Polyhach *et al*., 2011).

Electrophysiology

Planar lipid bilayers were formed by painting a lipid solution of azolectin (type IV S from Sigma) across a 200 µm aperture in a polysulfonate cup (Warner Instruments) separating two chambers of 1 ml each. The final concentration of lipids was 45 mg ml^{-1} dissolved in decane. The *trans* chamber compartment was connected to the headstage input of a bilayer clamp amplifier (BC-535, Warner Instruments). The *cis* chamber was held at virtual ground. Voltages were applied to the planar lipid bilayers through Ag-AgCl electrodes connected to the chambers via agar/KCl bridges. Both *cis* and *trans* chamber solutions were composed of 1 M KCl, 10 mM HEPES, pH 7.4. Several microlitres of purified proteins diluted 2000-fold in 1% octyl-polyoxyethylene were added to the *cis*-compartment. Recorded single-channel currents were filtered at 1 kHz and digitized at 4 kHz. Data acquisition was performed by using Digidata 1440A and Axoscope 10.2 (Molecular Devices), and the recordings were analysed by using Clampfit 10.2 (Molecular Devices). The three major conductance states (O1 to O3) of wt FhaC were taken into account using threshold event detection mode. Open probabilities (Po), current amplitudes and conductance values were analysed from 15 s to 60 s recordings at ± 20 mV only when one channel level was observed. All value analyses were done using Prism 6.0 (GraphPad). The results are expressed as mean ± standard error of the mean.

Other techniques

The secretion assays were performed in *E. coli* as described (Delattre *et al*., 2011), except that Fha60 was used as the model substrate. pItac138NM2lkH was introduced together with a pFc3 derivative into *E. coli* UT5600. The culture supernatants and membrane extracts were analysed by immunoblotting following 3 h of induction with IPTG using anti-FHA

and anti-FhaC antibodies, respectively (Delattre *et al.*, 2011; Guerin *et al.*, 2014), and the Fha60/FhaC ratio was determined. For the detection of *in vivo* S-S bonds, the pFc3 variants were introduced into *E. coli* JCB571 (*dsbA*::kan) (Bardwell *et al.*, 1991). After liquid cultures, the cell pellets were treated with 5 mM of N-Ethylmaleimide (Sigma) and then with SDS-PAGE loading buffer with or without a reducing agent. The proteins were analysed by immunoblotting. For the PEG-ylation reactions, *E. coli* cultures as above were harvested, rinsed with PBS and resuspended in 300 µl PBS containing 30 µM Mal-PEG-5K (Creative PEGwork). The reactions were carried out at room temperature for 1 h without stirring. Cells were then harvested by centrifugation, washed twice with PBS and resuspended in sample buffer without β-mercaptoethanol. Conjugates were analysed by immunoblotting following SDS-PAGE under non-reducing conditions. The antibiotic sensitivity assays were performed as described (Clantin *et al.*, 2007) using the indicated pFc3 derivatives.

Acknowledgements

We thank Maelenn Delcourt and Emmanuelle Petit for technical help and the IR RENARD FR3443 for the spectrometers. JG received a predoctoral scholarship from the Institut Pasteur de Lille and the Région Nord-Pas de Calais. The work was supported by the grant ANR-10-BLAN-1306 DYN FHAC to FJD.

References

Alsteens, D., Martinez, N., Jamin, M., and Jacob-Dubuisson, F. (2013) Sequential unfolding of Beta helical protein by single-molecule atomic force microscopy. *PLoS ONE* **8:** e73572.

Arnold, T., Zeth, K., and Linke, D. (2010) Omp85 from the thermophilic cyanobacterium *Thermosynechococcus elongatus* differs from proteobacterial Omp85 in structure and domain composition. *J Biol Chem* **285:** 18003–18015.

Bardwell, J.C.A., McGovern, K., and Beckwith, J. (1991) Identification of a protein required for disulfide bond formation *in vivo*. *Cell* **67:** 581–589.

Baud, C., Guerin, J., Petit, E., Lesne, E., Dupre, E., Locht, C., and Jacob-Dubuisson, F. (2014) Translocation path of a substrate protein through its Omp85 transporter. *Nat Commun* **5:** 5271. doi: 10.1038/ncomms6271.

Bennion, D., Charlson, E.S., Coon, E., and Misra, R. (2010) Dissection of beta-barrel outer membrane protein assembly pathways through characterizing BamA POTRA 1 mutants of *Escherichia coli*. *Mol Microbiol* **77:** 1153–1171.

Bos, M.P., Robert, V., and Tommassen, J. (2007) Functioning of outer membrane protein assembly factor Omp85 requires a single POTRA domain. *EMBO Rep* **8:** 1149–1154.

Clantin, B., Delattre, A.S., Rucktooa, P., Saint, N., Meli, A.C., Locht, C., *et al.* (2007) Structure of the membrane protein FhaC: a member of the Omp85-TpsB transporter superfamily. *Science* **317:** 957–961.

Delattre, A.S., Clantin, B., Saint, N., Locht, C., Villeret, V., and Jacob-Dubuisson, F. (2010) Functional importance of a conserved sequence motif in FhaC, a prototypic member of the TpsB/Omp85 superfamily. *FEBS J* **277:** 4755–4765.

Delattre, A.S., Saint, N., Clantin, B., Willery, E., Lippens, G., Locht, C., *et al.* (2011) Substrate recognition by the POTRA domains of TpsB transporter FhaC. *Mol Microbiol* **81:** 99–112.

Dwyer, R.S., Ricci, D.P., Colwell, L.J., Silhavy, T.J., and Wingreen, N.S. (2013) Predicting functionally informative mutations in *Escherichia coli* BamA using evolutionary covariance analysis. *Genetics* **195:** 443–455.

Fan, E., Fiedler, S., Jacob-Dubuisson, F., and Muller, M. (2012) Two-partner secretion of gram-negative bacteria: a single beta-barrel protein enables transport across the outer membrane. *J Biol Chem* **287:** 2591–2599.

Gruss, F., Zahringer, F., Jakob, R.P., Burmann, B.M., Hiller, S., and Maier, T. (2013) The structural basis of autotransporter translocation by TamA. *Nat Struct Mol Biol* **20:** 1318–1320.

Guedin, S., Willery, E., Tommassen, J., Fort, E., Drobecq, H., Locht, C., and Jacob-Dubuisson, F. (2000) Novel topological features of FhaC, the outer membrane transporter involved in the secretion of the *Bordetella pertussis* filamentous hemagglutinin. *J Biol Chem* **275:** 30202–30210.

Guerin, J., Baud, C., Touati, N., Saint, N., Willery, E., Locht, C., *et al.* (2014) Conformational dynamics of protein transporter FhaC: large-scale motions of plug helix. *Mol Microbiol* **92:** 1164–1176.

Hagan, C.L., Silhavy, T.J., and Kahne, D.E. (2011) beta-Barrel membrane protein assembly by the bam complex. *Annu Rev Biochem* **80:** 189–210.

Heinz, E., and Lithgow, T. (2014) A comprehensive analysis of the Omp85/TpsB protein superfamily structural diversity, taxonomic occurrence, and evolution. *Front Microbiol* **5:** 370. doi: 10.3389/fmicb.2014.00370.

Hodak, H., Clantin, B., Willery, E., Villeret, V., Locht, C., and Jacob-Dubuisson, F. (2006) Secretion signal of the filamentous haemagglutinin, a model two-partner secretion substrate. *Mol Microbiol* **61:** 368–382.

Hubbell, W.L., McHaourab, H.S., Altenbach, C., and Lietzow, M.A. (1996) Watching proteins move using site-directed spin labeling. *Structure* **4:** 779–783.

Jacob-Dubuisson, F., Villeret, V., Clantin, B., Delattre, A.S., and Saint, N. (2009) First structural insights into the TpsB/Omp85 superfamily. *Biol Chem* **390:** 675–684.

Jacob-Dubuisson, F., Guerin, J., Baelen, S., and Clantin, B. (2013) Two-partner secretion: as simple as it sounds? *Res Microbiol* **164:** 583–595.

Jansen, K.B., Baker, S.L., and Sousa, M.C. (2015) Crystal structure of BamB bound to a periplasmic domain fragment of BamA, the central component of the beta-Barrel assembly machine. *J Biol Chem* **290:** 2126–2136.

Jeschke, G. (2002) Distance measurements in the nanometer range by pulse EPR. *Chemphyschem* **3:** 927–932.

Jeschke, G., Chechik, V., Ionita, P., Godt, A., Zimmermann, H., Banham, J., *et al.* (2006) DeerAnalysis2006 – a comprehensive software package for analyzing pulsed ELDOR data. *Appl Magn Reson* **30:** 473–498.

Kim, S., Malinverni, J.C., Sliz, P., Silhavy, T.J., Harrison, S.C., and Kahne, D. (2007) Structure and function of an essential component of the outer membrane protein assembly machine. *Science* **317:** 961–964.

Leonard-Rivera, M., and Misra, R. (2012) Conserved residues of the putative L6 loop of *Escherichia coli* BamA play

a critical role in the assembly of beta-Barrel outer membrane proteins, including that of BamA itself. *J Bacteriol* **194:** 4662–4668.

Maier, T., Clantin, B., Gruss, F., Dewitte, F., Delattre, A.S., Jacob-Dubuisson, F., *et al*. (2015) Conservation of the Omp85 lid lock motif confirmed by a high-resolution structure of FhaC. *Nat Commun* **6:** 7452. doi: 10.1038/ncomms8452.

Mallarino, L.E., Fan, E., Odermatt, M., Müller, M., Lin, M., Liang, J., *et al*. (2015) TtOmp85, a beta-barrel assembly protein, functions by barrel augmentation. *Biochemistry* **54:** 844–852.

Méli, A.C., Hodak, H., Clantin, B., Locht, C., Molle, G., Jacob-Dubuisson, F., and Saint, N. (2006) Channel properties of TpsB transporter FhaC point to two functional domains with a C-terminal protein-conducting pore. *J Biol Chem* **281:** 158–166.

Ni, D., Wang, Y., Yang, X., Zhou, H., Hou, X., Cao, B., *et al*. (2014) Structural and functional analysis of the beta-barrel domain of BamA from *Escherichia coli*. *FASEB J* **28:** 2677–2685.

Noinaj, N., Kuszak, A.J., Gumbart, J.C., Lukacik, P., Chang, H., Easley, N.C., *et al*. (2013) Structural insight into the biogenesis of beta-barrel membrane proteins. *Nature* **501:** 385–390.

Noinaj, N., Kuszak, A.J., Balusek, C., Gumbart, J.C., and Buchanan, S.K. (2014) Lateral opening and exit pore formation are required for BamA function. *Structure* **22:** 1055–1062.

Noinaj, N., Rollauer, S.E., and Buchanan, S.K. (2015) The beta-barrel membrane protein insertase machinery from Gram-negative bacteria. *Curr Opin Struct Biol* **31:** 35–42.

Norell, D., Heuck, A., Tran-Thi, T.A., Gotzke, H., Jacob-Dubuisson, F., Clausen, T., *et al*. (2014) Versatile in vitro system to study translocation and functional integration of bacterial outer membrane proteins. *Nat Commun* **5:** 5396. doi: 10.1038/ncomms6396.

Polyhach, Y., Bordignon, E., and Jeschke, G. (2011) Rotamer libraries of spin labelled cysteines for protein studies. *Phys Chem Chem Phys* **13:** 2356–2366.

Ricci, D.P., Hagan, C.L., Kahne, D., and Silhavy, T.J. (2012) Activation of the *Escherichia coli* beta-barrel assembly machine (Bam) is required for essential components to interact properly with substrate. *Proc Natl Acad Sci USA* **109:** 3487–3491.

Rigel, N.W., Schwalm, J., Ricci, D.P., and Silhavy, T.J. (2012) BamE modulates the *Escherichia coli* beta-barrel assembly machine component BamA. *J Bacteriol* **194:** 1002–1008.

Rigel, N.W., Ricci, D.P., and Silhavy, T.J. (2013) Conformation-specific labeling of BamA and suppressor analysis suggest a cyclic mechanism for beta-barrel assembly in *Escherichia coli*. *Proc Natl Acad Sci USA* **110:** 5151–5156.

Schleiff, E., Maier, U.G., and Becker, T. (2011) Omp85 in eukaryotic systems: one protein family with distinct functions. *Biol Chem* **392:** 21–27.

Selkrig, J., Leyton, D.L., Webb, C.T., and Lithgow, T. (2014) Assembly of beta-barrel proteins into bacterial outer membranes. *Biochim Biophys Acta* **1843:** 1542–1550.

Stoll, S., and Schweiger, A. (2006) EasySpin, a comprehensive software package for spectral simulation and analysis in EPR. *J Magn Reson* **178:** 42–55.

Tellez, R., Jr, and Misra, R. (2012) Substitutions in the BamA beta-barrel domain overcome the conditional lethal phenotype of a DeltabamB DeltabamE strain of *Escherichia coli*. *J Bacteriol* **194:** 317–324.

Tikhonov, Y., and Arsenin, V. (1977) *Solutions of Ill-Posed Problems*. New York: John Wiley & Sons.

van Ulsen, P., Rahman, S., Jong, W., Daleke-Schermerhorn, M., and Luirink, J. (2014) Type V secretion: from biogenesis to biotechnology. *Biochim Biophys Acta* **1843:** 1592–1611.

Webb, C.T., Heinz, E., and Lithgow, T. (2012) Evolution of the beta-barrel assembly machinery. *Trends Microbiol* **20:** 612–620.